Journal of Fluorescence, Vol. 11, No. 3, September 2001 (© 2001)

Dynamics in Diether Lipid Bilayers and Interdigitated Bilayer Structures Studied by Time-Resolved Emission Spectra, Decay Time and Anisotropy Profiles

R. Hutterer[1] and M. Hof[2,3]

We present a comparative fluorescence spectroscopic investigation of diacyl and diether phosphatidylcholine vesicles using different probes with well-defined localization within either the hydrophilic headgroup region or the hydrophobic part of the bilayer. Time-resolved emission spectra have been used to characterize the solvent relaxation behavior in both symmetric and asymmetric diether and diacyl phosphatidylcholines. It is shown that time-resolved emission spectra of Prodan (6-propionyl-2-(dimethylamino)-naphthalene) and its long-alkyl chain derivative Patman (6-palmitoyl-2-[[trimethylammoniumethyl]methylamino]-naphthalene chloride) are a sensitive tool for the detection of differences in the micropolarities and viscosities at the hydrophobic/hydrophilic membrane interface of diether and diacyl lipids, respectively. Moreover, a new approach for the detection of interdigitated bilayers is discussed. It relies on the construction of anisotropy and decay time profiles for the set of *n*-anthroyloxy fatty acids and is compared with an older fluorescence assay based on intensity measurements only. The shape of plots of the fluorescence steady-state anisotropy versus the position of the chromophore (anthracene-9-carboxylic acid) combined with fluorescence lifetime measurements can be used to differentiate among non-fully, and mixed interdigitated gel phase structures and to predict structures for new lipid species.

KEY WORDS: Ether lipids; lipid interdigitation; solvent relaxation; time-resolved emission spectra; Prodan; Patman; *n*-anthroyloxy fatty acids.

INTRODUCTION

Fluorescence spectroscopy has contributed considerably to the present picture of the structure and function of biomembranes consisting predominantly of phospholipids. Among the fluorescence techniques employed such as quenching [1], energy transfer [2,3], lifetime (distributions) [4–6], and excimer formation [7,8], the determination of fluorescence anisotropy [4] has certainly been the dominating fluorescence method in studies of biological and model membranes. During the last few years, however, solvent relaxation monitored by fluorescence measurements has become a new, extremely useful method in biomembrane research [9].

The solvent relaxation technique allows for direct observation of viscosity and/or polarity changes in the close vicinity of the probe molecule that can be intentionally located in the hydrophobic backbone or in the hydrophilic headgroup region of the phospholipid bilayer. Such dyes described in recent publications were based on 2-amino-substituted naphthalene [10,11] and anthracene-9-carboxylic acid [12]. Representative 2-amino-substituted naphthalenes are the dye Prodan (6-propionyl-2-(dimethylamino)-naphthalene) and its long-alkyl chain derivative Patman (6-palmitoyl-2-[[trimethylammoniumethyl]

[1] Institute of Analytical Chemistry, Chemo- and Biosensors, University of Regensburg, D-93040 Regensburg, Germany.
[2] J. Heyrovský Institute of Physical Chemistry, ASCR, and Center for Complex Molecular Systems and Biomolecules, 18223 Prague 8, Czech Republic.
[3] To whom correspondence should be addressed. E-mail: Hof@jh-inst.cas.cz

1053-0509/01/0900-0227$19.50/0

methylamino]-naphthalene chloride), whose chromophores are known to be located within the hydrophilic headgroup region of the membrane. The *n*-anthroyloxy fatty acids (n-AS), on the other hand, constitute a unique set of fluorescent dyes for the hydrophobic backbone part of the membrane, with the great advantage of using a common chromophore (anthracene-9-carboxylic acid) which is covalently attached at different positions (n = 2, 6, 9, 12, 16) along the acyl chain of the fatty acid (stearic acid for n = 2–12, palmitic acid for n = 16). The n-AS probes are known to insert into the membrane with the stearoyl chains parallel to the phospholipid acyl chains, with the long axes of the anthroyl ring on average almost-perpendicular to the plane of the membrane [13]. The chromophore is positioned at a defined depth of the bilayer as confirmed by both ^{1}H-NMR [14] and quenching studies using Ca^{2+} and dimethylamine [15].

The benefit of the solvent relaxation approach in biomembrane research can be well demonstrated by listing membrane parameters influencing the solvent relaxation kinetics of a fluorescent label deposited in the membrane: membrane curvature and composition, addition of calcium ions, temperature, and protein binding [9–12]. Since the solvent relaxation method cannot be considered as a standard fluorescence technique up to know, its principles are briefly outlined in the first part of this review.

Although phospholipids containing ether-linked alkyl or 1-alkenyl chains have been widely found in various biological systems such as mammalian cell membranes and microorganisms [16], their functions are mostly unknown. Recent studies [17–20] have concentrated mainly on mono-ether lipids, which are thought to play an important role in pathobiochemistry, whereas little work has been done on diether lipids. This class of lipids differs only with regard to the chemical bonding between glycerol and the hydrophobic chains. One way to learn about their biological function is to investigate the potential change in physicochemical properties of membranes by enhanced levels of ether phospholipids, since the absence of a hydration bond partner may change the molecular packing in the headgroup domain. This approach provided the motivation to exploit the solvent relaxation monitored using Prodan and Patman for the characterization of the headgroup mobilities of vesicles containing monoether lipids [21,22] as well as asymmetric [23] and symmetric diether [24] lipids. In the second part of this review we summarize recent investigations employing the polarity-sensitive probes Prodan and Patman in lipid bilayers composed of both symmetric [1,2-dipalmitoyl-*sn*-glycero-3-phosphatidylcholine (DPPC) versus 1,2-dihexadecyl-*sn*-glycero-3-phosphatidylcholine (DHPC)] and strongly asymmetric [1-stearoyl-2-lauroyl-*sn*-glycero-3-phosphatidylcholine (DAPC) and 1-stearyl-2-lauryl-*sn*-glycero-3-phosphatidylcholine (DEPC)] phospholipids.

In the third part of this review we focus on another interesting property of diether lipids, i.e., their tendency to form interdigitated bilayer structures. Such interdigitated bilayer structures have attracted considerable interest with regard to both the different bilayer structures involved and their possible implications for membrane function. Three types of interdigitation have been observed, depending on the lipid structure, i.e., fully, mixed, and partially interdigitated bilayers. Fully interdigitated bilayers can occur in systems composed of lipids with either little or no chain asymmetry or in systems with the highest possible degree of asymmetry, including lysolipid species [25]. For saturated like-chain diacyl phosphatidylcholines the presence of amphiphilic compounds is usually required to induce the interdigitated $L_\beta I$ phase. Much work has been done on the induction of this phase by ethanol [26–32], but the $L_\beta I$ phase can also be adopted in the presence of higher alcohols [33], benzyl alcohol, ethylene glycol [34–36], chlorpromazine [35], thiocyanate ions [36], and polymyxin B [37]. Symmetric diether lipids such as DHPC, in contrast, show a fully interdigitated bilayer structure in the absence of any inducer [38–40]. The second type, called mixed interdigitation, is less common and results when the difference between the *sn*-1 and *sn*-2 acyl chains is about half as long as the length of the longer acyl chain [34,41]. This mixed interdigitation is characterized by the long acyl chain extending completely across the bilayer, whereas the two shorter chains meet end to end in the bilayer midplane. DAPC is an example of a phospholipid which forms a mixed interdigitated bilayer in the gel phase. Finally, a partially interdigitated bilayer packing mode exists in which the shorter chain from one monolayer pairs with the longer from the opposing monolayer. This arrangement has been proposed for medium asymmetric lipids such as 1-stearoyl-2-myristoyl-*sn*-glycero-3-phosphatidylcholine [34,39,42]. For the detection of interdigitation, X-ray diffraction [29,34–36,38,42–45] and neutron diffraction [46] are the most direct methods allowing direct evaluation of bilayer thickness [47,48]. However, infrared and Raman spectroscopy [49,50], electron spin resonance [51,52], differential scanning calorimetry (DSC) [27,38,39,53], NMR [54–56], and fluorescence spectroscopy [28,30,32,53] have also been used to detect and to study interdigitated lipid phases. Unfortunately, a drawback of the most informative diffraction methods is the large amount of material and the expensive facilities required. Simpler and faster methods requiring less mate-

rial, i.e., providing a higher sensitivity, are therefore desirable. Although a few fluorescence approaches have been described for the study of EtOH-induced bilayer interdigitation, a drawback of those assays is that they rely on changes in fluorescence intensity, which can monitor only transitions from one gel phase to another phase. Therefore we developed a new and simple method to distinguish normal bilayers (composed of diacyl lipids) and interdigitated bilayers (as formed by diether lipids in the gel phase) by fluorescence anisotropy and lifetime profiles, which are described in the third part of this review.

FLUORESCENCE SPECTROSCOPIC CHARACTERIZATION OF SOLVENT RELAXATION

The fluorescent probes used in solvent relaxation studies are characterized by a large change in the dipole moment $\Delta\mu$ [$\Delta\mu = \mu(S_1) - \mu(S_0)$] upon electronic excitation from the ground state S_0 to the excited state S_1. Since the time scale of the electronic transition is much shorter than that of nuclear motion, the excitation causes an ultrafast change in the probe's charge distribution but does not affect the position or orientation of the surrounding solvent molecules. The solvent molecules are, thus, forced to adapt to the new situation and start to reorient themselves to find an energetically favored position with respect to the excited dye. The dynamic process starting from the originally created nonequilibrium Franck–Condon state (F) and gradually establishing a new equilibrium in the excited state (R) is called solvent relaxation (SR). This relaxation results in a continuous red shift of the probe's emission spectrum from the emission maximum frequency of the Franck–Condon state [$\nu(0)$ for $t = 0$] to the emission maximum of the fully relaxed R state [$\nu(\infty)$ for $t = \infty$]. Since a more polar solvent typically leads to a stronger stabilization of the polar R state, the overall shift $\Delta\nu$ [$\Delta\nu = \nu(0) - \nu(\infty)$] increases with increasing solvent polarity for a given change of the solute's dipole moment $\Delta\mu$. The accurate mathematical description of this relationship depends on the choice of the dielectric solvation theories [57–64] and is not further considered here. For dielectric relaxation in phospholipid/water systems, it can be concluded that changes in $\Delta\nu$ directly reflect polarity changes in the dye environment, giving the first major information provided by the solvent relaxation technique in membrane studies.

The second information obtainable from the measurement of time-dependent spectral shifts is based on the fact that the SR kinetics is determined by the mobility of the dye environment. The response of solvent molecules to the electronic rearrangement of the dye is fastest in the case of water: more than half of its overall solvation response occurs under 55 femtoseconds (fs) [65]. If the dye is located in a viscous medium such as phospholipid membranes, the solvent relaxation takes place on the nanosecond (ns) time scale [66]. In vitrified solutions, on the other hand, the dye may fluoresce before solvent relaxation toward the R state is completed [67]. The time evolution of the solvation energy relaxation process can be described by means of the normalized spectral response function or so-called "correlation function" $C(t)$:

$$C(t) = \frac{\nu(t) - \nu(\infty)}{\Delta\nu} \tag{1}$$

The development of ultrafast spectroscopic methods with fs resolution has led to an accurate determination of $C(t)$ for a large variety of polar solvents and has allowed physical interpretation within the framework of existing theoretical models [65,68–70]. Some experimental results of several research groups have been summarized in a recent review [9].

The $C(t)$ function is usually determined by "spectral reconstruction" [71] of time-resolved emission spectra (TRES) from wavelength-dependent time-resolved decay data. The individual wavelength-dependent decays obtained at regular intervals across the emission spectrum are fitted to a sum of exponentials until a mathematically satisfactory fit is obtained [72]. The TRES at a given time t, $S(\lambda;t)$, is obtained by the fitted decays, $D(t;\lambda)$, by relative normalization to the steady-state spectrum, $S_0(\lambda)$, as follows:

$$S(\lambda;t) = \frac{(D(t;\lambda) \times S_0(\lambda))}{\int_0^\infty (D\ (t;\lambda)\ dt} \tag{2}$$

After conversion from a wavelength representation to one linear in frequency, the TRES are fit by the empirical "log-normal function" [73], which gives a realistic picture of broad, asymmetric electronic emission bands [74]. Should the log-normal model fail to fit the data, excited-state processes other than pure continuous solvent relaxation may be considered. From the fitted spectra the emission maximum frequencies $\nu(t)$, the total Stokes shift $\Delta\nu$, and the full width at half-maximum of the TRES ("half-width") are usually derived. Since $\nu(t)$ contains information about both the polarity ($\Delta\nu$) and the viscosity of the reported environment, the spectral shift $\nu(t)$ is normalized to the total shift $\Delta\nu$. The resulting "correlation functions" $C(t)$[Eq. (1)] describe the time course of the solvent response and allow for comparison of the SR

kinetic and, thus, of the relative microviscosities, reported from environments of different polarities.

It has to be kept in mind that the $C(t)$ function results from several arithmetical operations treating measured fluorescence decays and an emission spectrum; thus, experimental errors can multiply. When applying the SR technique in anisotropic media such as membranes, it must be considered that the dye might probe a distribution of microenvironments; in this case $C(t)$ might represent a continuous superposition of several solvent responses. In all investigations on membrane labels done by our group employing a subnanosecond "single-photon counting" apparatus [8,10–12,23,24] the solvent response appears to be rather complex and cannot be satisfactorily and consistently described by (multi)exponential relaxation models. To characterize the overall time scale of the solvation response, we therefore omit data fitting and use an (integral) average relaxation time:

$$\langle \tau_r \rangle \equiv \int_0^\infty C(t)dt \qquad (3)$$

SOLVENT RELAXATION IN DIETHER LIPIDS

The dynamic behavior of phospholipids containing ether-linked alkyl or 1-alkenyl chains has been studied in considerably less detail compared to diacyl lipids, although their participation in biological processes is beyond doubt. Most work has been done on ether lipids of the plasminogen type [1-*O*-(1′-*Z*-alkenyl)-2-acetyl-*sn*-glycero-3-phospholipids], especially their derivatives containing choline or ethanolamine bound to the phosphate. The latter may be found in nerve tissue, kidney, bone marrow, and red blood cells, while muscle cells and bone marrow constitute major sources of choline plasmalogens [75–77]. Ether lipids are thought to be involved in the pathobiochemistry of malignant tumor growth, where enhanced concentrations of ether lipids have been reported to be associated with neoplastic tissue [78,79]. Important pathophysiological functions such as stimulation of platelet aggregation and antihypertensive activity have been attributed to the activity of 1-*O*-(1′-*Z*-alkenyl)-2-acetyl-*sn*-glycero-3-phosphatidylcholine, the so-called platelet-activating factor. Although the molecular difference between diacyl and diether phosphatidylcholines may be regarded as small (an ester group is substituted by an ether oxygen), the absence of a hydrogen bond partner may significantly change the molecular packing and the solvation dynamics in the headgroup domain. In the following we summarize recent investigations employing the polarity-sensitive probes Prodan and Patman in lipid bilayers composed of both symmetric (DPPC versus DHPC) and strongly asymmetric (DAPC and DEPC) phosphatidylcholines.

Fluorescence decays of Patman and Prodan in all four pure lipid systems [small unilamellar vesicles (SUV) and large unilamellar vesicles (LUV) for symmetric and asymmetric lipids, respectively] as well as in a 1:1 mixture of DAPC and DEPC (LUV) have been recorded as a function of emission wavelength for several characteristic temperatures and fitted to biexponential decay models. Typically, for $\lambda_{em} > 470$ nm one decay component was obtained with a negative preexponential factor which is characteristic for the occurrence of an excited-state reaction. A large increase in the decay times can be observed with increasing λ_{em}, as expected for increasing contributions of excited states. For all temperatures the mean decay times are significantly shorter in the corresponding diether lipid (DEPC, DHPC) compared to the diacyl lipid (DAPC, DPPC). The mixed lipid system DAPC/DEPC (1:1) yields decay times close to the mean of those detected for DAPC and DEPC. To obtain a more quantitative picture of solvent relaxation TRES, Stokes shifts $\Delta\nu$ versus time after excitation, correlation functions $C(t)$, and half-widths of the reconstructed TRES have been examined for all the above-mentioned lipid systems labeled with either Prodan or Patman. Briefly, they give direct evidence that the ether linkage allows more efficient water penetration in the glycerol region, resulting in faster SR.

Some representative data are summarized in the following. First, Prodan exhibits faster SR than Patman, irrespective of the lipid system, in agreement with its localization closer to the lipid–water interface [10]. Second, the SR of both dyes becomes faster with increasing amounts of diether lipid. Below or near the phase transition, the relaxation of Patman is very slow in diacyl lipids, while it is still fast in diether lipids. The same trend, but with considerably shorter relaxation times, holds above the phase transition in DAPC and DEPC. Similar conclusions can be drawn from a comparison of symmetrical diacyl and diether lipids (DPPC and DHPC).

Some illuminating data are compiled in Table I for Patman in DPPC- and DHPC-SUV. It is shown that the total time-dependent Stokes shifts in DPPC-SUV below T_m are relatively small (5 and 17 nm for 20 and 40°C, respectively), whereas the shifts in DHPC at these temperatures are considerably larger (31 and 43 nm, respectively). Apparently, the ether linkage leads to a more polar environment and, thus, in the given phospholipid/water system, to a more efficient water penetration. The correlation functions $C(t)$ (Fig. 1) and the determined $\langle \tau_r \rangle$

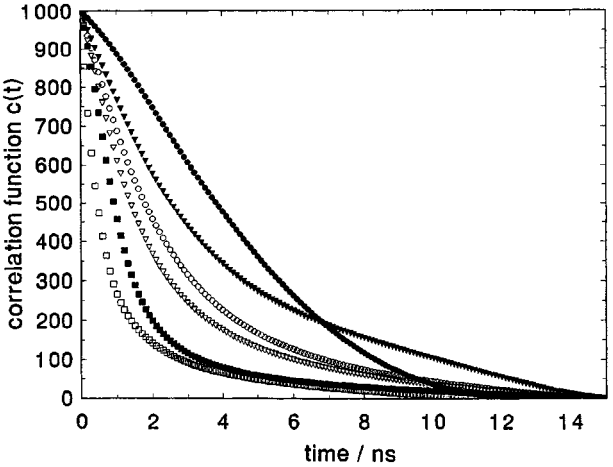

Fig. 1. Correlation functions $C(t)$, calculated according to Eq. (1), for Patman in DPPC-SUV (filled symbols) and DHPC-SUV (open symbols) at 20°C (circles), 40°C (triangles), and 52°C (squares).

(Table I) confirm for all temperatures the above-stated conclusion that the headgroup domain probed by Patman is more mobile in the case of ether compared with acyl membranes. It has to be stressed that the $C(t)$ for DPPC at 20°C or for DHPC at 52°C may be insignificant because of its small shift or the large contribution of solvent relaxation faster than the time resolution of the experiment, respectively. Anyhow, both $C(t)$ values are included in Fig. 1 to visualize the solvent relaxation kinetics of these systems.

The very slow solvent relaxation in DPPC below T_m as well as the very fast solvent relaxation in DHPC above T_m manifest themselves in the time course of the TRES half-widths (Fig. 2): If the fluorescence lifetime is long enough to allow complete relaxation to the R state, the half-width of the TRES first increases to a maximum, usually at times comparable to $\langle\tau_r\rangle$, and then decreases with time [68,80–82]. This regular behavior is found for Patman probing DHPC-SUV below T_m as well as for the DPPC system above T_m. The observed profiles of half-width versus time after excitation for these three investigated systems indicate that, during the lifetime of the excited-state, solvent relaxation is completed and that the major part of the solvent relaxation process is detectable with the given subnanosecond time resolution of the experiment. The continuous increase observed for DPPC-SUV below T_m indicates that Patman fluoresces before SR is complete. The opposite extreme is observed for DHPC above T_m: the maximum in the half-width is already present at very short times after excitation. Together with the surprising drop in the determined $\Delta\nu$ for DHPC to 31 nm at 52°C, it can be concluded that a major part of the SR occurs much faster than the time resolution of the experiment and, thus, cannot be detected with the given time resolution.

Similar conclusions have been reached for the monoether lipids 1-*O*-hexadec-1′-enyl-2-oleoyl-*sn*-glycero-3-phosphatidyl choline (HOPC) and 3-*O*-hexadecyl-2-oleoyl-*sn*-glycero-3-phosphatidyl choline (AOPC) in comparison to POPC (1-palmitoyl-2-oleoyl-*sn*-glycero-3-phosphatidyl choline) [21]. The idea of a more flexible molecular environment [21] is in agreement with ^{2}H NMR data showing enhanced flexibility of the α-methylene segment of the *sn*-2 chain of a plasmine plasmalogene compared to the corresponding diacyl lipid [83]. A stronger penetrance of water due to a less steep dielectric gradient along the hydrophobic/hydrophilic interface in plasmalogenes has been postulated [75] and appears to be even more pronounced in diether lipids.

As shown previously [24] by steady-state anisotropy measurements with Patman and the well-known DPH

Table I. Stokes Shifts (Δλ) and Mean Relaxation Times ($\langle\tau_r\rangle$) (ns) for Patman in DPPC- and DHPC-SUV[a]

Temperature (°C)	DPPC, T_m = 41°C		DHPC, T_m = 43°C	
	$\langle\tau_r\rangle$ (ns)	Δλ (nm)	$\langle\tau_r\rangle$ (ns)	Δλ (nm)
20	(ND)	5	2.6	31
40	3.7	17	2.0	43
52	1.2	49	<0.7	>31

[a] The $\langle\tau_r\rangle$ for DPPC at 20°C was not determined (ND) because of the small Stokes shift in this system. The limited time resolution used in the single-photon counting experiment allowed the determination of only threshold values of Δλ and $\langle\tau_r\rangle$ for DHPC-SUV at 52°C (see also the discussion of Fig. 2). T_m is the lipid phase transition temperature.

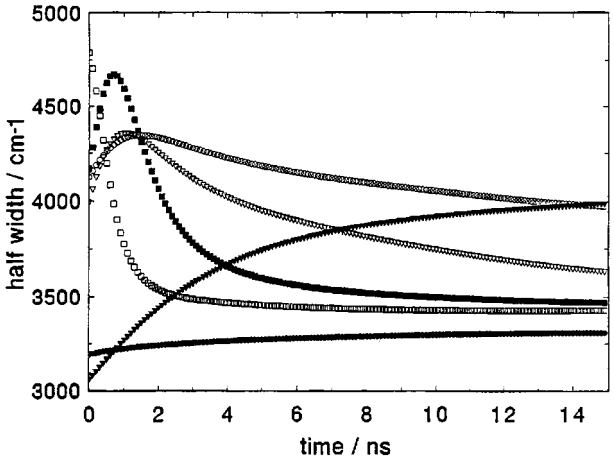

Fig. 2. Full width at half-maximum of the TRES ("half-width") as a function of time after excitation for Patman in DPPC-SUV (filled symbols) and DHPC-SUV (open symbols) at 20°C (circles), 40°C (triangles), and 52°C (squares).

derivative TMA-DPH [1-(4-trimethylammonium-phenyl)-6-phenyl-1,3,5-hexatriene], the differences in the relaxation behavior are not caused by different fluorophore mobilities in diacyl and diether lipids but rather by different physical properties of the interface region. To summarize this section, TRES has been proven to be a sensitive tool for the detection of differences in reorientation of phospholipid headgroups and/or water dipols in the hydrophobic/hydrophilic membrane interface.

DETECTION OF INTERDIGITATED GEL PHASES BY ANISOTROPY AND LIFETIME PROFILES

In recent years it has been recognized that, besides the classic bilayer arrangement, another gel phase structure is possible in which the acyl chains of opposing monolayers interdigitate. Three types of bilayer interdigitation have been reported and are described briefly in the Introduction. Despite the need for a fast and simple assay to detect bilayer interdigitation, only very few fluorescence approaches based on either pyrene [84] or DPH fluorescence have been described. The latter used by Nambi *et al.* to study EtOH-induced interdigitation of DPPC bilayers relies on intensity changes of the DPH fluorescence [28]. Monitoring the steady-state intensities of DPH in DPPC, the authors observed an abrupt decrease in fluorescence intensity of DPH when the EtOH concentration reached a value sufficient to induce transition to a fully interdigitated phase. A drawback of techniques based on changes in fluorescence intensity is that they give information only about the fact that a phase transition occurred but are not able to give any information about the lipid organization of the two phases involved. This limitation can be overcome by the use of an extensive parameter such as decay time or anisotropy rather than an intensive one such as intensity.

A useful approach is discussed in the following to obtain anisotropy profiles, i.e., a set of values for the steady-state anisotropy as a function of fluorophore position along the bilayer normal [85]. The set of n-AS dyes is ideally suited for such a task due to their defined localization in lipid bilayers. In the case that the phase behavior (and thus transition temperature) of a lipid under study is not known, it is useful to measure first the steady-state anisotropy (r_{ss}) as a function of temperature for the full set of n-AS dyes. These data can be used to construct profiles of the steady-state anisotropy versus the position of the chromophore along the acyl chain for some characteristic temperatures and will typically yield a kind of fluidity gradient along the bilayer normal. The approach has been used to compare the symmetric diacyl lipid DPPC (forming "normal" bilayers) with the symmetric diether lipid DHPC, using multilamellar vesicles (MLV) [85]. For DHPC, a fully interdigitated structure has been confirmed by X-ray and differential scanning calorimetry [39] which converts to a "normal" gel phase at 34.5°C and to the liquid crystalline phase at 43.5°C. The second pair was DMPC and DAPC (MLV) [85], the latter favoring a mixed interdigitated bilayer structure below 18.5°C [42]. In a normal gel phase the differences in the steady-state anisotropies for the set of n-AS dyes are generally quite small, with 16-AP exhibiting the lowest values. All fluorophores show a pronounced decrease in the r_{ss} values near the main phase transition, which is largest for the dyes located closer to the bilayer center (9- and 12-AS, 16-AP). In DHPC the temperature dependence of the steady-state anisotropy is quite different. Considerably higher r_{ss} values are obtained for 2-AS and 3-AS and, especially, 16-AP at low temperatures compared to the noninterdigitated phase in DPPC. Thus, 16-AP is more restricted in the fully interdigitated phase compared to the normal gel phase in DPPC. The behavior is again quite different for the asymmetric DAPC, known to adopt a mixed interdigitated gel phase ($L_\beta I$) below T_m with three acyl chains per headgroup. While a clear fluidity gradient is observed from 2-AS to 12-AS, 16-AP exhibits the highest r_{ss} values of all dyes examined (0.243) in the gel phase of DAPC, with an abrupt decrease to the lowest value above T_m.

Profiles of the steady-state anisotropy versus the position of the chromophore along the acyl chain are shown in Figs. 3A and B for some characteristic reduced temperatures. The noninterdigitated gel phases are characterized by a small rise in anisotropy from position 2 to position 6, followed by a steady decrease in r_{ss} down to position 16. A pronounced fluidity gradient from position 2 to position 16 is characteristic for the liquid crystalline phase (diamonds) of all investigated lipids. Higher anisotropies for 2- and 3-AS and a continuous decrease down to position 12 characterize the mixed interdigitated phase. The most intriguing feature, however, is the extraordinary high anisotropy values for 16-AP in the mixed interdigitated phase, which are much higher than in a "normal" (i.e., noninterdigitated) gel phase. A similar profile is observed for the fully interdigitated phase at low temperatures. Again, the r_{ss} values are high for 2- and 3-AS but considerably lower for 6-, 9-, and 12-AS. In contrast to the noninterdigitated phase (DPPC), a considerable rise in r_{ss} is observed from 12-AS to 16-AP. This profile changes markedly at higher temperatures. At 32°C the maximal anisotropy is observed for 3-AS,

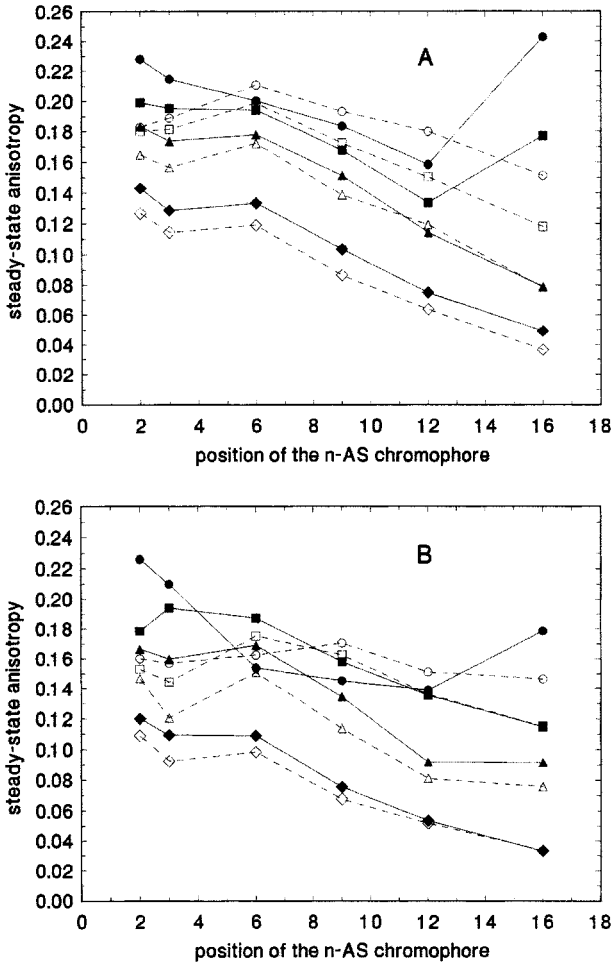

Fig. 3. Steady-state anisotropy profiles of n-AS dyes in DMPC-MLV (open symbols) and DAPC-MLV (filled symbols) (**A**) and in DPPC-MLV (open symbols) and DHPC-MLV (filled symbols) (**B**). Plots are shown for the same reduced temperatures relative to the phase transition. (**A**) Filled symbols: 5°C (circles), 14°C (squares), 18°C (triangles), and 30°C (diamonds). Open symbols: 10°C (circles), 19°C (squares), 23°C (triangles), and 35°C (diamonds). (**B**) Filled and open symbols: 10°C (circles), 32°C (squares), 42°C (triangles), and 50°C (diamonds).

followed by 6-AS, with a continuous decrease from 6-AS to 16-AP. Above T_m, the profile is similar to those of the other lipids.

Thus, each of the three examined gel phase types (noninterdigitated, mixed interdigitated, and fully interdigitated) yields a different characteristic profile, which seems to be of diagnostic value for the determination of the packing type of a specific lipid. This has been shown by examination of the steady-state anisotropy for the set of n-AS in MLV composed of the asymmetric diether lipid DEPC. To our knowledge, no X-ray diffraction data for the gel phase structure of this lipid have been published yet. As with DAPC, a very high value is obtained for 2-AS at a low temperature (5°C), with decreasing values in the series 3- ≈ 6- > 9-> 12-AS. From 12-AS to 16-AP a pronounced increase was detected, which is indicative of an interdigitated structure.

Within this set of probes, 16-AP is clearly the most useful and interesting one. Its extremely different behavior in DMPC, DHPC, and DAPC is summarized in Fig. 4. Very high anisotropies are observed in the mixed interdigitated phase in both MUV and LUV (data not shown). In contrast, considerably lower values were observed in SUV, indicating that the formation of a mixed interdigitated phase is not possible in small vesicles due to geometrical constraints.

Of course, the method is also useful for the study of other lipid systems which are known to exhibit interdigitation, such as the induction of a fully interdigitated phase of DPPC by EtOH mentioned above. A set of r_{ss} data at 20°C for the n-AS dyes versus the ethanol concentration (Fig. 5A) and the corresponding anisotropy profiles exhibit no major changes up to 1.0 *M* EtOH. However, the anisotropies change markedly between 1.0 and 1.4 *M* EtOH, which is exactly the concentration range in which the transition to the fully interdigitated phase of DPPC was reported to occur [28,29]. The anisotropy profile obtained at 1.9 *M* EtOH (Fig. 5B) is typical for a fully interdigitated phase, as may be seen by comparison with the profile for DHPC at 10°C (Fig. 3B).

The power of the method using a set of n-AS dyes for the simple assessment of the type of lipid gel phase structure can be improved if additional decay time measurements are performed. It is well known that the lifetimes of n-AS dyes are sensitive to polarity [12,15,86], while

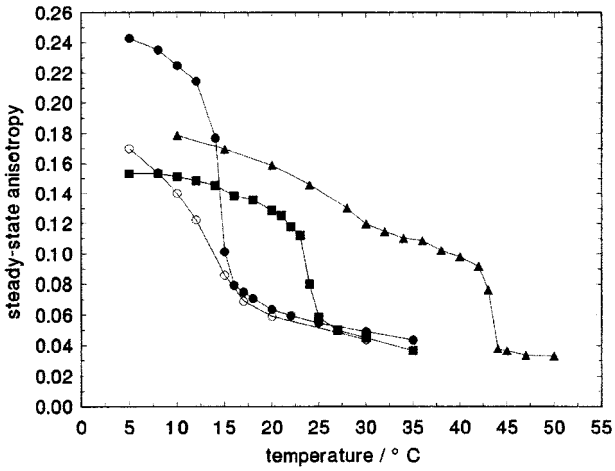

Fig. 4. Steady-state anisotropies as a function of temperature of 16-AP in DAPC-MLV (filled circles), DAPC-SUV (open circles), DHPC-MLV (triangles), and DMPC-MLV (squares). The excitation wavelength was 385 nm; emission was detected at 430 nm.

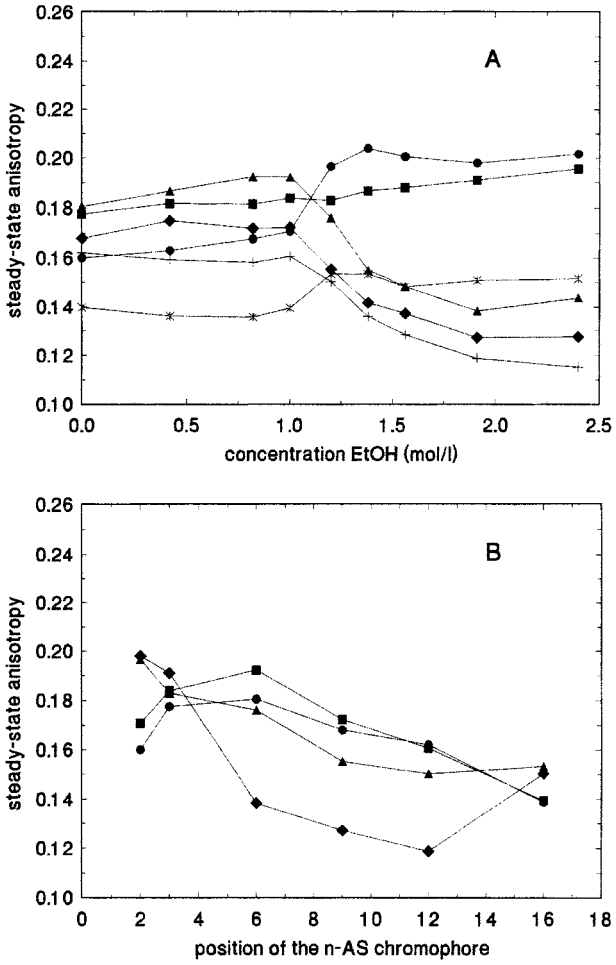

Fig. 5. Steady-state anisotropies of n-AS in DPPC-MLV at different EtOH concentrations. (**A**) Plots of the steady-state anisotropy as a function of the EtOH concentration. The excitation wavelength was 385 nm; emission was detected at 430 nm. The temperature was 20°C. Circles, 2-AS; squares, 3-AS; triangles, 6-AS; diamonds, 9-AS; crosses, 12-AS; stars, 16-AP. (**B**) Anisotropy profiles of n-AS dyes in DPPC-MLV for different EtOH concentrations: circles, 0 *M*; squares, 1.0 *M*; triangles, 1.2 *M*; diamonds, 1.9 *M* EtOH.

for interdigitated bilayers a lower polarity gradient has been proposed [52]. Recent studies have shown that the relaxation behavior of anthroyloxy fatty acids in phospholipid vesicles is somewhat more complex than previously assumed. For a detailed discussion of these features the reader is referred to Ref. 12. Nevertheless, the fluorescence decay at 430 nm appears to be a good indicator for the polarity gradient within the bilayer [87]. It can be well described by a biexponential decay for all dyes. The mean decay times, calculated according to

$$\langle\tau\rangle = (\alpha_1\tau_1^2 + \alpha_2\tau_2^2)/(\alpha_1\tau_1 + \alpha_2\tau_2) \qquad (4)$$

where $a_{1/2}$ are the preexponential factors of both components, increase from 2-AS to 16-AP in a normal bilayer system such as DPPC. If the mean lifetime of 2-AS is taken as 100% and the decay times of the other n-AS dyes are expressed as the percentage increase relative to 2-AS, characteristic profiles for the decay behavior in different bilayer arrangements can be obtained [85]. A comparison of the noninterdigitated DPPC with the fully interdigitated (below 34.5°C) DHPC (MLV) shows considerably smaller increases in the mean decay times of n-AS with increasing depths of incorporation in DHPC, in agreement with a fully interdigitated structure with a smaller bilayer thickness.

The most interesting feature of the decay behavior in the mixed interdigitated phase of DAPC is the unique behavior of 16-AP. Its decay behavior is close to monoexponential, with an extremely long decay time of about 17 ns in the gel phase contributing more than 90% to the total fluorescence intensity. To our knowledge such a long decay component for 16-AP has never been reported for any other vesicle system. Above 15°C, 16-AP shows an abrupt decrease in decay time (from 15.0 ns at 15°C to 13.4 ns at 17°C and, further, to 12.5 ns at 25°C), which is very similar to that in DMPC at the same reduced temperature (12.4 ns). Thus, the transition from the mixed interdigitated to the liquid crystalline state is accompanied by a drastic change in the environment of 16-AP.

Similarly the very long decay time for 16-AP in DEPC at temperatures below the phase transition supported the assumed existence of a mixed interdigitated gel phase structure for this diether lipid. Mean decay times above 15.0 ns as found for both DAPC and DEPC are unique and seem to be associated with a mixed interdigitated bilayer. No obvious explanation for the origin of the uniquely long lifetime of 16-AP in mixed interdigitated structures is currently available. Due to the reduced bilayer thickness of the interdigitated phase compared to DMPC, the 16-AP chromophore should be localized close to the lipid/water interface, sensing an environment of considerable polarity if an all-trans conformation for the palmitoyl chain is assumed. As the decay times for the n-AS decrease with increasing polarity, a much shorter decay time than observed experimentally would be expected. One possible explanation is that 16-AP loops back into the bilayer to avoid the exposure of the hydrophobic aromatic ring to the polar lipid/water interface. This may allow a position in a highly restricted environment where little quenching occurs and which seems not to be favored in a fully interdigitated gel phase. It should be mentioned that the terminal position of the anthroyl group represents an anomaly in the series of *n*-anthroyloxy fatty acids, which may generally cause deviations in the fluorescence behavior.

CONCLUSION

Although differing only slightly in structure from the more common diacyl phosphatidylcholines, bilayers composed of diether phosphatidylcholines have been shown to exhibit distinctly different physical properties. TRES can reveal considerably faster solvent relaxation and more efficient water penetration for diether phosphatidylcholines, especially in the liquid crystalline phase. Diether lipids such as DHPC form fully interdigitated gel phase structures at low temperatures. A simple method to differentiate different types of gel phase structures using fluorescence spectroscopy has been summarized. Obviously, fluorescence data can yield only indirect information on structural features; thus X-ray diffraction techniques will remain indispensable for the unambiguous determination of lipid phase structures. Nevertheless, it seems remarkable how much information can be derived by relatively simple fluorescence anisotropy measurements, especially if additional decay time measurements are performed. The shapes of plots of the steady-state anisotropy versus the position of the fluorophore combined with lifetime measurements for 16-AP can be used to differentiate non-, fully, and mixed interdigitated gel phase structures and to predict structures for new lipid species.

ACKNOWLEDGMENT

This work was supported by Research Grant 203/99/0845 from the Grant Agency of the Czech Republic.

REFERENCES

1. M. R. Eftink (1992) in J. R. Lakowicz (Ed.), *Topics in Fluorescence Spectroscopy; Principles*, Plenum Press, New York, p. 53.
2. B. W. Van der Meer, G. Coker, and S. Y. S. Chen (1994) *Resonance Energy Transfer Theory and Data*, VCH Verlag, Weinheim.
3. R. Hutterer, K. Krämer, F. W. Schneider, and M. Hof (1997) *Chem. Phys. Lipids* **90**, 11.
4. C. D. Stubbs and B. W. Williams (1992) in J. R. Lakowicz (Ed.), *Topics in Fluorescence Spectroscopy: Biochemical Applications*, Plenum Press, New York, p. 231.
5. C. Bernsdorff, A. Wolf, R. Winter, and E. Gratton (1997) *Biophys. J.* **72**, 1264.
6. K. Brand, M. Hof, and F. W. Schneider (1991) *Ber. Bunsenges. Phys. Chem.* **95**, 1511.
7. G. Duportail and P. Lianos (1996) in M. Rosoff (Ed.), *Vesicles*, Marcell Dekker, New York, p. 296.
8. R. Hutterer, A. Haefner, F. W. Schneider, and M. Hof (1997) in J. Slavik (Ed.), *Fluorescence Microscopy and Fluorescence Probes, Vol. 2*, Plenum Press, New York.
9. M. Hof (1999) in W. Rettig *et al.* (Eds.), *Solvent Relaxation in Biomembranes (Applied Fluorescence in Chemistry, Biology, and Medicine)*, Springer Verlag, Berlin, pp. 139–456.
10. R. Hutterer, F. W. Schneider, H. Sprinz, and M. Hof (1996) *Biophys. Chem.* **61**, 151–60.
11. R. Hutterer, F. W. Schneider, W. T. Hermens, R. Wagenvoord, and M. Hof (1998) *Biochim. Biophys. Acta* **1414**, 155–164.
12. R. Hutterer, F. W. Schneider, H. Lanig, and M. Hof (1997) *Biochim. Biophys. Acta* **1323**, 195–207.
13. S. R. Jones, R. I. Willing, K. R. Thulborn, and W. H. Sawyer (1979) *Chem. Phys. Lipids* **24**, 11.
14. F. Podo and J. K. Blasie (1972) *Proc. Natl. Acad. Sci. USA* **69**, 1032.
15. K. R. Thulborn and W. H. Sawyer (1978) *Biochim. Biophys. Acta* **511**, 125.
16. F. Paltauf (1983) in H. K. Mangold and F. Paltauf (Eds.), *Ether Lipids: Biochemical and Biomedical Aspects*, Academic Press, New York, pp. 309–353.
17. D. O. Shaw and J. M. Shulman (1965) *J. Lipid Res.* **6**, 341.
18. A. Hermetter and F. Paltauf (1981) *Chem. Phys. Lipids* **29**, 225.
19. D. J. Vaughan and K. M. Keough (1974) *FEBS Lett.* **47**, 158.
20. D. J. Siminovitch, M. J. Ruocco, and R. G. Griffin (1984) *Biophys. J.* **45**, 197a.
21. A. Sommer, F. Paltauf, and A. Hermetter (1990) *Biochemistry* **29**, 11134.
22. A. Hermetter, E. Prenner, J. Loidl, E. Kalb, A. Sommer, and F. Paltauf (1993) in O. S. Wolfbeis (Ed.), *Fluorescence Spectroscopy*, Springer Verlag, Berlin, p. 149.
23. R. Hutterer, F. W. Schneider, V. Fidler, E. Grell, and M. Hof (1997) *J. Fluoresc.* **7**, 161.
24. R. Hutterer, F. W. Schneider, and M. Hof (1997) *J. Fluoresc.* **7**, 27.
25. J. L. Slater and C. Huang (1988) *Prog. Lipid Res.* **27**, 325–359.
26. E. S. Rowe (1992) in R. Watson (Ed.), *Alcohol: Neurobiology and Physiology*, CRC Press, Boca Raton, FL, pp. 239–267.
27. E. S. Rowe and T. A. Cutrera (1990) *Biochemistry* **29**, 10398–10404.
28. P. Nambi, E. S. Rowe, and T. J. McIntosh (1988) *Biochemistry* **27**, 9175–9182.
29. S. A. Simon and T. J. McIntosh (1984) *Biochim. Biophys. Acta* **773**, 169–172.
30. H. Komatsu and E. S. Rowe (1991) *Biochemistry* **30**, 2463–2470.
31. J. Zeng, K. E. Smith, and P. L.-G. Chong (1993) *Biophys. J.* **65**, 1404–1414.
32. M. Yamazaki, M. Miyazu, and T. Asano (1992) *Biochim. Biophys. Acta* **1106**, 94–98.
33. E. S. Rowe and J. M. Campion (1994) *Biophys. J.* **67**, 1888–1895.
34. R. V. McDaniel, T. J. McIntosh, and S. A. Simon (1983) *Biochim. Biophys. Acta* **731**, 97–108.
35. T. J. McIntosh, R. V. McDaniel, and S. A. Simon (1983) *Biochim. Biophys. Acta* **731**, 109–114.
36. B. A. Cunningham and L. J. Lis (1986) *Biochim. Biophys. Acta* **861**, 237–242.
37. A. Theretz, J. L. Ranck, and J. F. Tocanne (1983) *Biochim. Biophys. Acta* **732**, 499–508.
38. M. J. Ruocco, D. J. Siminovitch, and R. G. Griffin (1985) *Biochemistry* **24**, 2406–2411.
39. P. Laggner, K. Lohner, G. Degovics, K. Müller, and A. Schuster (1987) *Chem. Phys. Lipids* **44**, 31–60.
40. J. T. Kim, J. Mattay, and G. G. Shipley (1987) *Biochemistry* **26**, 6592–6598.
41. H. Xu and C. Huang (1987) *Biochemistry* **26**, 1036–1043.
42. J. Mattai, P. K. Sripada, and G. G. Shipley (1987) *Biochemistry* **26**, 3287–3297.
43. E. N. Serrallach, R. Dijkman, G. H. De Haas, and G. G. Shipley (1983) *J. Mol. Biol.* **170**, 155–174.
44. S. W. Hui, J. T. Mason, and C. Huang (1984) *Biochemistry* **23**, 5570–5577.
45. J. L. Ranck and J. F. Tocanne (1982) *FEBS Lett.* **143**, 175–177.
46. L. F. Braganza and D. L. Worcester (1986) *Biochemistry* **25**, 2591–2596.
47. N. P. Franks and Y. K. Levine (1981) in E. Grell (Ed.), *Membrane Spectroscopy*, Springer Verlag, pp. 437–487.

48. N. P. Franks and W. R. Lieb (1981) in C. G. Knight (Ed.), *Liposomes: From Physical Structure to Therapeutic Application*, Elsevier/North Holland, Biochemical Press, Amsterdam, pp. 243–272.
49. T. J. O'Leary and I. W. Levine (1984) *Biochim. Biophys. Acta* **776**, 185–189.
50. C. Huang, J. T. Mason, and I. W. Levin (1983) *Biochemistry* **22**, 2775–2780.
51. J. M. Boggs, G. Rangaraj, and A. Watts (1989) *Biophys. Biochim. Acta* **981**, 243–253.
52. J. M. Boggs and G. Rangaraj (1985) *Biochim. Biophys. Acta* **816**, 221–233.
53. Y. L. Kao, P. L.-G. Chong, and C. Huang (1990) *Biophys. J.* **58**, 947–956.
54. M. J. Ruocco, A. Makriyannis, D. J. Siminovitch, and R. G. Griffin (1985) *Biochemistry* **24**, 4844–4851.
55. J. Frenzell, K. Arnold, and P. Nuhn (1978) *Biochim. Biophys. Acta* **507**, 185–197.
56. D. J. Siminovitch, K. R. Jeffrey, and H. Eibl (1983) *Biochim. Biophys. Acta* **727**, 122–134.
57. B. Bagchi, S. D. Oxtoby, and G. R. Fleming (1984) *Chem. Phys.* **86**, 257.
58. I. Rips, J. Klafter, and J. Jortner (1988) *J. Chem. Phys.* **89**, 4288.
59. I. Rips, J. Klafter, and J. Jortner (1988) *J. Chem. Phys.* **88**, 3246.
60. H. L. Friedman, F. O. Raineri, F. Hirata, and P. C. Perng (1995) *J. Stat. Phys.* **78**, 239.
61. F. O. Raineri, H. L. Friedman, and P. C. Perng (1994) *Chem. Phys.* **183**, 187.
62. N. G. Bakshiev (1964) *Opt. Spectosc. (USSR)* **16**, 446.
63. Y. T. Mazurenko and N. G. Bakshiev (1970) *Opt. Spectosc. (USSR)* **28**, 490.
64. W. Liptay (1974) in E. C. Lim (Ed.), *Excited States*, Academic Press, New York, Vol. 1, p. 129.
65. R. Jimenez, G. R. Fleming, P. V. Kumar, and M. Maroncelli (1994) *Nature* **369**, 471.
66. S. Mukherjee and A. Chattopadhyay (1995) *J. Fluoresc.* **5**, 237.
67. M. Hof and P. Lianos (1997) *Langmuir* **13**, 290.
68. M. L. Hornig, J. A. Gardecki, A. Papazyan, and M. Maroncelli (1995) *J. Phys. Chem.* **99**, 17320.
69. H. Zhang, A. M. Jonkman, van der Meulen, and M. Glasbeek (1994) *Chem. Phys. Lett.* **236**, 587.
70. D. Bingemann and N. P. Ernsting (1995) *J. Chem. Phys.* **102**, 2691.
71. M. Maroncelli and G. R. Fleming (1987) *J. Chem. Phys.* **86**, 6221.
72. M. Hof, J. Schleicher, and F. W. Schneider (1989) *Ber. Bunsenges. Phys. Chem.* **93**, 1377.
73. D. B. Siano and D. F. Metzler (1969) *J. Chem. Phys.* **51**, 1856.
74. E. W. Castner Jr., M. Maroncelli, and G. R. Fleming (1987) *J. Chem. Phys.* **86**, 1090.
75. A. Hermetter (1988) *Comments Mol. Cell. Biophys.* **5**, 133.
76. G. Rouser and A. Yamamoto (1968) *Lipids* **3**, 284.
77. W. T. Norton (1981) *Adv. Neurol.* **31**, 93.
78. B. V. Howard, J. De B. Butler, and J. M. Bailey (1973) in R. Wood (Ed.), *Tumor Lipids: Biochemistry and Metabolism*, Am. Oil Chem. Soc. Press, Champaign, IL, pp. 200–214.
79. F. Spener (1983) in H. K. Mangold and F. Paltauf (Eds.), *Ether Lipids, Biochemical and Biomedical Aspects*, Academic Press, New York, pp. 239–259.
80. R. Richert and A. Wagener (1991) *J. Phys. Chem.* **95**, 10115.
81. M. Maroncelli (1993) *J. Mol. Liq.* **57**, 1.
82. M. Vincent, J. Galley, and A. P. Demchenko (1995) *J. Phys. Chem.* **99**, 14923.
83. M. Malthaner, A. Hermetter, F. Paltauf, and J. Seelig (1987) *Biochim. Biophys. Acta* **900**, 191.
84. M. Yamazaki, M. Miyazu, and T. Asano (1992) *Biochim. Biophys. Acta* **1106**, 94–98.
85. R. Hutterer, F. W. Schneider, and M. Hof (1997) *Chem. Phys. Lipids* **86**, 51–64.
86. K. R. Thulborn, L. M. Tilley, W. H. Sawyer, and F. E. Treolar (1979) *Biochim. Biophys. Acta* **558**, 166–172.
87. K. Brand (1993) *Ph.D. thesis*, University of Wuerzburg, Wuerzburg.